Journal of Medicinal Chemistry

Article

pubs.acs.org/jmc

Structural Basis for the Accommodation of Bis- and Tris-Aromatic Derivatives in Vitamin D Nuclear Receptor

Fabrice Ciesielski,[†] Yoshiteru Sato,[‡] Yassmine Chebaro, Dino Moras, Annick Dejaegere, and Natacha Rochel*

Institut de Génétique et de Biologie Moléculaire et Cellulaire (IGBMC), Institut National de Santé et de Recherche Médicale (INSERM) U964, Centre National de Recherche Scientifique (CNRS) UMR 7104, Université de Strasbourg, 67404 Illkirch, France

Supporting Information

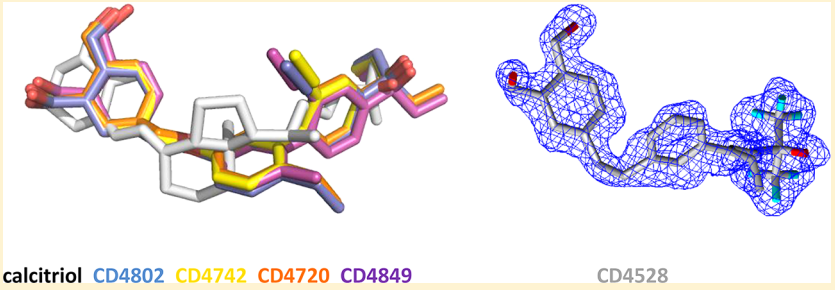

ABSTRACT: Actual use of the active form of vitamin D (calcitriol or 1α,25-dihydroxyvitamin D_3) to treat hyperproliferative disorders is hampered by calcemic effects, hence the continuous development of chemically modified analogues with dissociated profiles. Structurally distinct nonsecosteroidal analogues have been developed to mimic calcitriol activity profiles with low calcium serum levels. Here, we report the crystallographic study of vitamin D nuclear receptor (VDR) ligand binding domain in complexes with six nonsecosteroidal analogues harboring two or three phenyl rings. These compounds induce a stimulated transcription in the nanomolar range, similar to calcitriol. Examination of the protein−ligand interactions reveals the mode of binding of these nonsecosteroidal compounds and highlights the role of the various chemical modifications of the ligands to VDR binding and activity, notably (de)solvation effects. The structures with the tris-aromatic ligands exhibit a rearrangement of a novel region of the VDR ligand binding pocket, helix H6.

INTRODUCTION

1α,25-Dihydroxyvitamin D_3 [1α,25$(OH)_2D_3$] or calcitriol (Figure 1), the biologically most active form of vitamin D_3, binds to the vitamin D receptor (VDR), a member of the nuclear receptor superfamily. Calcitriol regulates multiple biological functions including cell growth, differentiation, antiproliferation, apoptosis, adaptive/innate immune responses, bone mineralization, and calcium/phosphate homeostasis.[1−3] Deregulation of VDR action may lead to severe diseases such as cancers, psoriasis, rickets, renal osteodystrophy, and autoimmunity (multiple sclerosis, rheumatoid arthritis, inflammatory bowel diseases, type I diabetes).[4,5] Thus, VDR may be a therapeutic target to cure patients.[6] The major drawbacks for the use of calcitriol as a drug to treat hyperproliferative disorders are undesired hypercalcemic effects. Therefore, it remains a major challenge to design analogues of 1α,25-dihydroxyvitamin D_3 that display dissociation between antiproliferative/prodifferentiating action and calcemic effects.[7] Among them, the steroidal superagonists with some modifications on the A and/or CD rings or aliphatic chain of the natural ligand mediate transcriptional activity with a magnitude at least 10-fold higher than the natural ligand with identical or lower calcemic properties.[8−10] Another group of analogues is composed of nonsecosteroidal ligands that mimic the natural calcitriol without direct structural relationship to calcitriol.[11−13] Few ligands of this type have been reported to activate VDR. There are currently five classes of nonsecosteroidal ligands. These include the diphenylmethane LG190178 (Figure 1) and its derivatives,[11−17] C/D modified analogues,[18] bis- and tris-aromatic derivatives,[19−21] podocarpic acid derivatives,[22] and natural bile acid and nutritional ligands.[23] Only some of the diphenylmethane derivatives and of the bis- and tris-aromatic derivatives have been shown to be potent VDR agonists.[11−17,19−21] Some of these nonsecosteroidal ligands present less calcium mobilization and are attractive therapeutics against psoriasis, osteoporosis, and cancer.[15,17,19−21] Nonsteroidal compounds for other steroidal NRs are currently used in cancer treatment such as raloxifene for estrogen receptor ER[24] or flutamide for androgen receptor AR.[25]

Structural studies of NRs have greatly contributed to the understanding of how ligand binding leads to the activation of NRs (reviewed in refs 26 and 27) and has helped to design new supergagonists VDR ligands.[9,11] In the present investigation, we describe the structure−function characterization of the nonsecosteroidal bis-aromatic (CD4528 and CD3938) and tris-

Received: June 19, 2012
Published: September 7, 2012

dx.doi.org/10.1021/jm300858s | J. Med. Chem. 2012, 55, 8440−8449

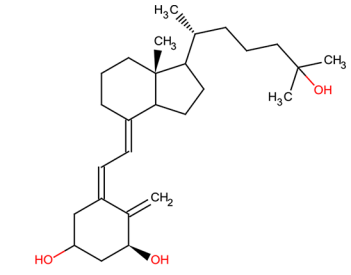

calcitriol

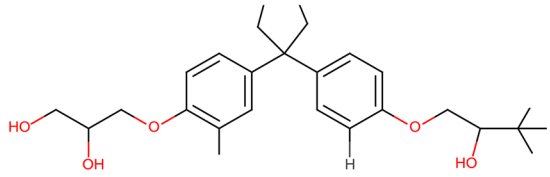

LG190178

Bis-aromatic

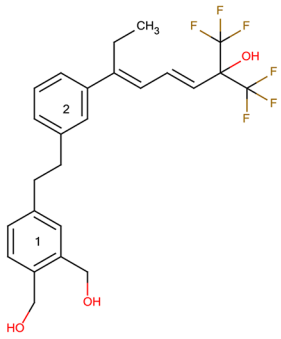

CD4528

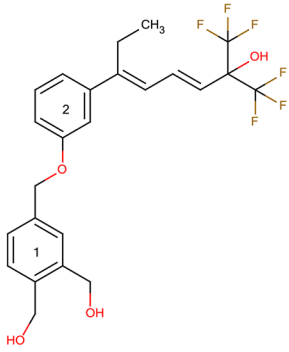

CD4420

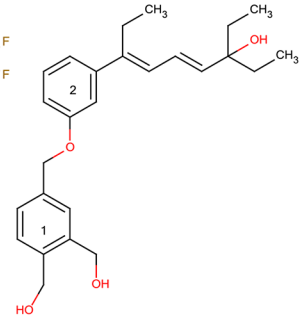

CD3938

Tris-aromatic

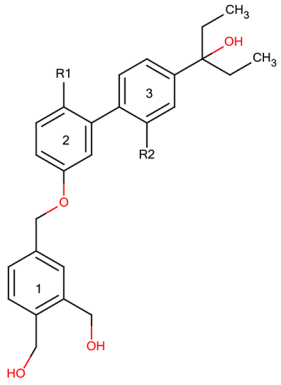

R1=methyl; R2=propyl CD4720
R1=ethyl; R2=ethyl CD4742
R1=ethyl; R2=propyl CD4802

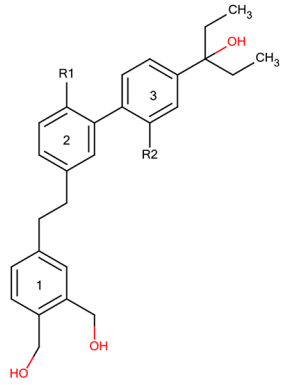

R1=methyl; R2=propyl CD4849

Figure 1. Chemical structures of calcitriol and the nonsecosteroidal analogues LG190178, the bis-aromatic derivatives CD4528, CD4020, and CD3938, and the tris-aromatic derivatives CD4720, CD4742, CD4802, and CD4849.

aromatic derivatives (CD4720, CD4742, CD4802, and CD4849) (Figure 1). These compounds induce a stimulated transcription from a VDR-response element in co-transfection assays with a similar potency as calcitriol. The crystal structures of the ligand binding domain of the human or zebrafish VDR in complexes with the bis-aromatic CD4528 and CD3938 and tris-aromatic derivatives CD4720, CD4742, CD4802, and CD4849 reveal that all the nonsecosteroidal derivatives maintain similar hydrogen binding network and hydrophobic interactions as the natural ligand. Increased stability of activation helix 12 of VDR is observed for the most potent ones.

RESULTS

Chemistry and Biological Evaluation. The common fragment of the studied bis- and tris-aromatic derivatives is the dibenzyl alcohol (phenyl ring 1, Figure 1). The second phenyl (phenyl ring 2) is either linked by ether (CD3938, CD4720, CD4742, and CD4802) or alkyl (CD4528 and CD4849) chains. For the bis-aromatic derivatives, a dienyl alcohol is branched to the second phenyl and the methyl moieties of the dienyl alcohol in CD4528 and CD4420 are replaced by trifluoromethyl. In the tris-aromatic derivatives, a third phenyl group (phenyl ring 3) is included in the branched side chain,

dx.doi.org/10.1021/jm300858s | J. Med. Chem. 2012, 55, 8440−8449

replacing the dienyl alcohol of the bis-aromatic analogues. These tris-aromatic derivatives vary by a series of alkyl chains in positions R1 and R2 in the second and third phenyl groups, respectively (Figure 1). R1 is either a methyl or ethyl, while R2 is either an ethyl or a propyl group. It was assumed that the length and the size of the substituent may modulate their biological activities. Their synthesis and biological evaluation were described in the patent literature.[20,21] The VDR dependent transcriptional activity was quantified using HeLa cells that were transiently co-transfected with hVDR full-length expression vector and the CYP24 luciferase reporter construct. Dose-response data provided the AC50 concentration that is the concentration of ligand for 50% activation response (Table 1).[20,21] The analogues exhibit a drastic difference in their capacity to induce transcription. Indeed, in the bis-aromatic series, CD4528 is the most potent ligand with transcription activity similar to that of the natural ligand. Replacing the ether linker (CD4420) between the two phenyl groups by an alkyl group (CD4528) increases the biological activity. For the tris-aromatic derivatives, the only ligand with an alkyl linker between the two first phenyl rings (CD4849) shows the highest transcriptional activity.

Table 1. Nonsecosteroidal Ligands CD4528, CD4802, and CD4849 Are Potent Transcriptional Activators of VDR[a]

ligand	AC_{50} (nM)[20,21]
calcitriol	2.5, 1[19]
CD3938	49
CD4528	2.8, 1.7[19]
CD4420	5[19]
CD4802	2.2
CD4849	0.5

[a] AC_{50} (activation concentration for 50% response) determined in HeLa cells.[20,21] Standard errors on AC_{50} are less than 5%.[20,21]

Crystal Structures. The ligand-binding domain of human VDR (hVDR, residues 118−427Δ166−216) and zebrafish VDR (zVDR, residues 156−453) were expressed in *E. coli*, purified, and crystallized in presence of 3 mol equiv of ligands. For zVDR, the complexes were crystallized in presence of SRC-1 coactivator peptide corresponding to the second LXXLL motif of SRC-1. All ligands were first tested for crystallization in complexes with hVDR LBD. However, only one ligand (CD4528) in complex with hVDR gave crystals usable for X-ray analysis. The other complexes were crystallized using the wild-type zVDR LBD. The zebrafish construct was previously used in order to circumvent the packing constraints of the unique crystal form obtained for the mutant human hVDR in which 50 residues containing insertion region between helices H2 and H3 have been deleted.[28] In both zVDR LBD/calcitriol and hVDR LBD/calcitriol structures, the conformation and interactions of the ligand are identical.[28,29] The hVDR complex crystallizes in $P2_12_12_1$ space group, while the zVDR complexes crystallize in $P6_522$ space group. The structures were solved by molecular replacement using the hVDR/calcitriol and zVDR/calcitriol structures as starting models. The data collection and refinement statistics of the structures of the zVDR/CD4528, zVDR/CD3938, zVDR/CD4720, zVDR/CD4742, zVDR/CD4802, and zVDR/CD4849 and of the hVDR/CD4528 complexes are summarized in Table 2. The overall structures are highly homologous to the VDR/calcitriol structures. All VDR complexes adopt the canonical active conformation observed for agonist bound receptors, similar to the zVDR/calcitriol and to the mutant hVDR/calcitriol complexes.[29] For the zVDR complexes, the insertion region between helices H2 and H3 present in the protein was disordered and was not visible in the electron density map. The position and conformation of the activation helix H12 in the zVDR complexes are strictly maintained, and the SRC-1 peptide forms an amphipatic α-helix interacting with the hydrophobic cleft formed by H3 and H4 through two hydrogen bonds with zGlu446 [hGlu420] and zLys274 [hLys246]. The residue's number in the text corresponds to the zVDR sequence zAAxxx with the corresponding human sequence numbers within brackets [hAAxxx]. Compared to the structure of hVDR/calcitriol complex, the atomic coordinates of all Cα-atoms of hVDR/CD4528 show a root-mean-square deviation (rmsd) of 0.29 Å. The atomic models of zVDR bound to CD3938, CD4528 CD4720, CD4742, CD4802, and CD4849 showed rmsd values on all Cα-atoms of 0.34, 0.30, 0.50, 0.54, 0.56, and 0.50 Å, respectively, when compared to the structure of the zVDR/calcitriol complex. For the last four complexes, a rearrangement of the protein is observed going from helix H6 through the β-sheet region and to a lesser extent for the loop between helices H1 and H3 (Supporting Information Figure 1). The rmsd values on the Cα atoms for the region of helix H6 (residues 316−330 of zVDR) are 1.11, 1.63, 1.85, and 1.31 Å for the zVDR/CD4720, zVDR/CD4742, zVDR/CD4802, and zVDR/CD4849 complexes, respectively, compared to zVDR/1α,25$(OH)_2D_3$. The corresponding values in the loop 1−3 are 0.65, 0.68, 0.77, and 0.61 Å, respectively.

Structural Accommodation of the Bis-Aromatic Derivatives CD3938 and CD4528. The two bis-aromatic derivatives, CD3938 and CD4528, do not induce a rearrangement of the main chain of the VDR LBD. The ligands are buried in the predominantly hydrophobic pocket that is conserved in all complexes (Figure 2). The ligand pocket is similar in size and shape to that of calcitriol (Supporting Information Table 1). The interactions between the receptor and the ligands involve both electrostatic and hydrophobic interactions. Electrostatic interactions mediated by hydroxyl groups are in particular extremely well conserved. The three hydroxyl groups of the CD3938 and CD4528 play the same roles as the 1-OH, 3-OH, and 25-OH of calcitriol and are hydrogen-bonded to VDR (Figure 2). In hVDR/CD4528, the 1-OH group interacts through hydrogen bonds with hSer237 and hArg274, the 2-OH group with hTyr143 and hSer278, and the 3-OH with hHis305 and hHis397. The positions of these hydrophilic groups induce some deviations of the side chains of the residues interacting through the hydrogen bonds (Figure 2). Schematic representations of the interactions between VDR and CD3938 and CD4528 are shown in Supporting Information Figures 2 and 3. The hydrophobic interactions in the region of the secosteroid involve the same residues for the two bis-aromatic ligands. The phenyl ring 1 of the two compounds occupies the same region in the VDR LBD as the A-ring of calcitriol. The second phenyl ring occupies the region of the C-ring of calcitriol for CD3938 and of the D-ring of calcitriol in the case of CD4528, while the side chain of phenyl ring 2 superposes to the alkyl side chain of calcitriol.

Even though the interactions with the receptor are globally very similar for the two compounds and for calcitriol, there are some differences between the two ligands. In particular, the second phenyl ring is perpendicular to the C/D rings of the natural ligand for CD3938 and is parallel in the case of CD4528

Table 2. Data Collection and Refinement Statistics

	zVDR						
	CD3938	CD4720	CD4742	CD4802	CD4849	CD4528	hVDRΔ CD4528
PDB code	4G1Y	4G1D	4G21	4G1Z	4G20	4G2H	4G2I
				Data Collection			
beamline	SLS PX	ID14-2	ID14-2	SLS PX	ID14-2	ID14-3	ID14-2
space group	$P6_522$	$P6_522$	$P6_522$	$P6_522$	$P6_522$	$P6_522$	$P2_12_12_1$
cell dimensions	$a = b = 65.559$ Å	$a = b = 66.652$ Å	$a = b = 66.287$ Å	$a = b = 66.472$ Å	$a = b = 66.497$ Å	$a = b = 66.438$ Å	$a = 44.741$ Å
	$c = 263.876$ Å	$c = 263.141$ Å	$c = 263.662$ Å	$c = 262.336$ Å	$c = 262.551$ Å	$c = 265.761$ Å	$b = 51.449$ Å
	$\alpha = \beta = 90°$	$\alpha = \beta = 90°$	$\alpha = \beta = 90°$	$\alpha = \beta = 90°$	$\alpha = \beta = 90°$	$\alpha = \beta = 90°$	$c = 132.427$ Å
	$\gamma = 120°$	$\gamma = 120°$	$\gamma = 120°$	$\gamma = 120°$	$\gamma = 120°$	$\gamma = 120°$	$\alpha = \beta = \gamma = 90°$
resolution (last shell) (Å)	20−2.85 (2.94−2.85)	20−2.7 (2.79−2.7)	20−2.9 (2.97−2.90)	20−2.5 (2.57−2.5)	20−2.9 (2.97−2.90)	25−2.5 (2.59−2.5)	20−1.8 (1.87−1.8)
unique reflections	7838	9462	7344	12014	7790	13007	25821
completeness (last shell) (%)	99.8 (98.9)	98.9 (93.7)	98 (96.1)	85.5 (81.6)	98.2 (90.7)	100 (100)	97.8 (95.6)
R_{sym} (last shell) (%)	5.1 (15.6)	5.4 (15.0)	6.0 (28)	5.4 (21.6)	6.0 (13.1)	6.6(43.8)	5.0 (35.9)
refinement (resolution)	20−2.85	20−2.7	20−2.9	15−2.5	20−2.9	25−2.5	20−1.8
R_{cryst} (%)	22.3	22.0	23.2	23.0	23.3	20.8	19.5
R_{free} (%)	28.3	28.4	29.1	27.9	28.7	28.5	22.3
rmsd bond length (Å)	0.006	0.005	0.006	0.006	0.01	0.005	0.005
rmsd angle (deg)	1.03	0.98	0.93	1.12	1.46	1.01	1.06

dx.doi.org/10.1021/jm300858s | J. Med. Chem. 2012, 55, 8440−8449

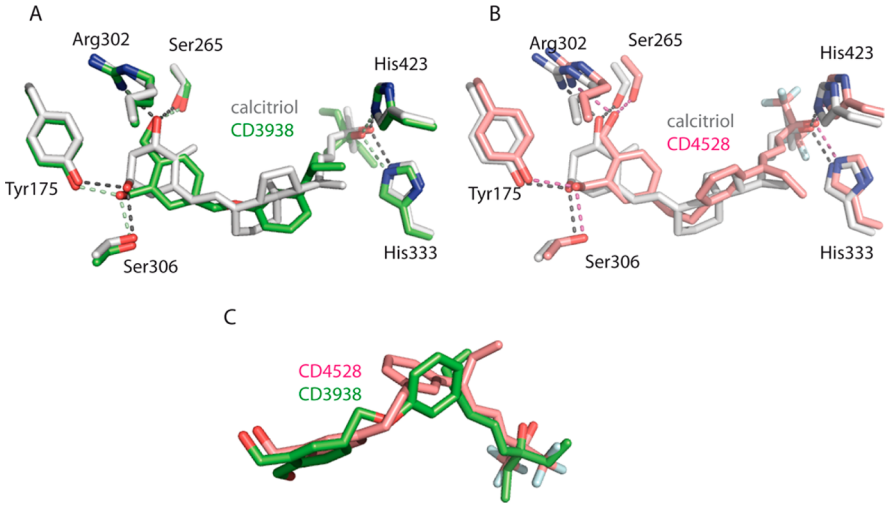

Figure 2. Conformations of the bis-aromatic analogues CD3938 and CD4528. (A) Superimposition of CD3938 (green) and calcitriol (gray) in the VDR LBP. (B) Superimposition of CD4528 (salmon) and calcitriol (gray) in the VDR LBP. Hydrogen bonds are shown by dotted lines. (C) The second phenyl rings of CD3938 and CD4528 adopt different conformations as shown by the superpimposition of CD3938 (green) and CD4528 (salmon) ligands after superimposed VDR complexes. Oxygen atoms are colored in red. Correspondence of residues numbers between human and zebrafish VDRs: hTyr143 (zTyr175), hSer237 (zSer265), hArg274 (zArg302), hSer278 (zSer 306), hHis305 (zHis333), and hHis397 (zHis423).

(Figure 2C). Although the resolution of the zVDR/CD3938 does not allow a detailed interpretation of these differences based on the crystal structure, it is interesting to note that the preferred conformation(s) of the flexible linker between ring 1 and 2 differs for a linker that contains an oxygen and one that contains only carbon atoms. Two model compounds [2-(hydroxymethyl)-4-(2-phenylethyl)phenyl]methanol (labeled ethyl) and [2-(hydroxymethyl)-4-(phenoxymethyl)phenyl]-methanol (labeled oxymethyl) were constructed and optimized ab initio in order to evaluate the minimum energy conformation and specifically the torsion angles of the linker region (Figure 3). Two conformations of the ethyl compound were considered corresponding to the ab initio optimized geometries of compounds CD4528 (labeled ethyl-4528) and CD4849 (labeled ethyl-4849) in the gas phase. The corresponding torsion angles (Table 3 and Figure 3) differ, in particular $C_{arom}-C_{arom}-O-C_{sp^3}$ with a local minimum at 180° and $C_{arom}-C_{arom}-C_{sp^3}-C_{sp^3}$ with a local minimum at 90°,

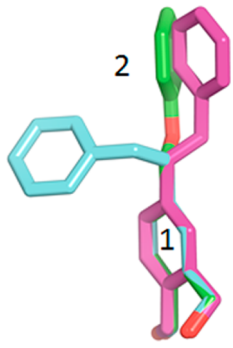

Figure 3. Superposed ab initio structures of the model compounds [2-(hydroxymethyl)-4-(2-phenylethyl)phenyl]methanol (labeled ethyl) and [2-(hydroxymethyl)-4-(phenoxymethyl)phenyl]methanol (labeled oxymethyl). Rings 1 and 2 are as in Figure 1. For the ethyl linker, two different local minima corresponding to the conformation of rings 1 and 2 in the optimized structures of compound CD4528 and compound CD4849 are displayed. For the oxymethyl linker, only one conformer was observed in the different crystal structures.

respectively. The ab initio geometry optimization of CD3938 and CD4528 indeed showed that the local conformation of the linker region in the VDR complex corresponds closely to a local gas phase energy minimum, with torsion angles close to the ethyl and oxymethyl model compounds (Table 4). The conservation of favored rotamers in the complexes indicates that the ligands are not strained, with no associated energetic penalty upon binding. As a result of these intrinsic conformational preferences of the linker and considering that rings 1 of both compounds are superposed, the orientation of ring 2 differs. However, VDR residues in this region of the binding pocket make rather loose contacts with phenyl ring 2 and accommodate the different orientations of the second phenyl ring without major reorganization. It must also be noted that compound CD4849 displays yet another combination of linker dihedral angles (Table 3 and Figure 3) that is accommodated in the VDR binding pocket as well.

The main differences between CD3938 and CD4528 are observed in the region of the aliphatic side chain. Some interactions are lost compared to calcitriol in the regions of the C/D rings and of the side chain (Supporting Information Figure 2). In the case of CD4528, only one interaction is lost at a 4 Å cutoff with hTyr323 while several new interactions are made through the fluorine atoms of the trifluoromethyl groups with hVal418 and hPhe422 of helix H12 and with hLeu414 of loop H11−H12 at a distance of 3.3 and 3.7 Å, respectively. As a consequence, helix H12 is more stabilized in the VDR/CD4528 complex.

Activity assays indicate that compound CD4528 is significantly more potent than compound CD3938 (Table 1). The two compounds differ in the presence of the fluoromethyl groups on the alkyl tail, which make different interactions with the receptors, and by the difference in linker between rings 1 and 2 (ethyl versus oxymethyl). As discussed above, the intrinsic conformational preferences of the two linkers do not seem to affect much the interactions of the two compounds with the receptor. Another factor that can affect the potency of ligands is the desolvation cost of polar groups, particularly if it is not compensated by polar interaction with the receptor. In

dx.doi.org/10.1021/jm300858s | J. Med. Chem. 2012, 55, 8440−8449

Table 3. Ab Initio Dihedral Angles of the Linker between Ring 1 and Ring 2 in the Model Compounds [2-(Hydroxymethyl)-4-(2-phenylethyl)phenyl]methanol (Labeled Ethyl) and [2-(Hydroxymethyl)-4-(phenoxymethyl)phenyl]methanol (Labeled Oxymethyl)[a]

	dihedral angle (deg)		
	$C_{ar2}-C_{ar2}-CH_2-CH_2$	$C_{ar}-CH_2-CH_2-C_{ar}$	$CH_2-CH_2-C_{ar1}-C_{ar1}$
ethyl-4528	99	−68	97
ethyl-4849	90	180	89
	dihedral angle (deg)		
	$C_{ar2}-C_{ar2}-O-CH_2$	$C_{ar2}-O-CH_2-C_{ar1}$	$O-CH_2-C_{ar1}-C_{ar1}$
oxymethyl	178	177	−45

[a]The aromatic carbon labels ar1 and ar2 refer to phenyl rings 1 and 2 (Figure 1). For the ethyl linker, dihedral angles are given for the two different local minima corresponding to the conformation ring 1−linker−ring 2 observed in the ab initio optimized geometries of compound CD4528 (ethyl-4528) and compound CD4849 (ethyl-4849). For the oxymethyl linker, only one conformer was observed in the crystal structures. The corresponding structures are given in Figure 3.

Table 4. Torsion Angles of the Linker Chain Connecting the Two Phenyl Groups of the Bis- and Tris-Derivatives in the Original Crystal Structures and the Ones Optimized ab Initio

	torsion angle (deg)	
compd	crystal structure	optimized ab initio
	Torsion Angle for $C_{ar}-CH_2-CH_2-C_{ar}$	
CD4528	−54	−67.5
CD4849	172.5	179.7
	Torsion Angle for $C_{ar}-O-CH_2-C_{ar}$	
CD3938	178.3	−175.9
CD4720	176.8	173.1
CD4742	178.2	177.3
CD4802	177.1	170.9

order to evaluate the supplemental desolvation cost of the oxymethyl linker with respect to the ethyl linker, we used ab initio reaction field methods to compare the solvation of three pairs of ligands that differ only in the composition of the linker: compounds CD4420 and CD4528, compounds CD4720 and CD4849 (Figure 1), and the model compounds ethyl and oxymethyl used previously (Figure 3). We focus on the electrostatic contribution to solvation most directly linked to the presence of oxygen versus carbon, and clearly for the three pairs of ligands compared, the desolvation cost of the compounds with the oxymethyl linker is higher than that of the corresponding compounds with the ethyl linker (Table 5). The magnitude of calculated difference ranges between 0.3 and 1.1 kcal/mol and could thus contribute a factor of 3−8 to the difference in affinities of the ligands for the receptor.

Table 5. Comparison of the Electrostatic Contribution to Solvation for Ligands That Differ Solely in the Composition of the Linker between Ring 1 and Ring 2 (Ethyl vs Oxymethyl)[a]

ligand	electrostatic solvation (kcal/mol)
CD4420	−14.7
CD4528	−14.4
CD4720	−14.3
CD4849	−13.1
ethyl	−9.5
oxymethyl	−10.6

[a]Calculations were done using ab initio reaction field as described in Experimental Section.

Structural Accommodation of the Tris-Aromatic CD4720, CD4742, CD4802, and CD4849. The conformations of the four ligands are similar with a superposition of the three phenyl rings as shown in Figure 4A. Compared to VDR/calcitriol complexes, the volumes of the ligand pocket are larger, in agreement with the increase in size of the ligands (Supporting Information Table 1). The dibenzyl alcohol of the tris-aromatic derivatives occupies the same region in the VDR LBD as the A-ring of calcitriol and has the same conformation as in the bis-aromatic derivatives (Figure 4B). All derivatives with an alkyl or ether linker between the dibenzyl alcohol and the second phenyl group exhibit a similar conformation of the second phenyl ring as shown by their torsion angles (Table 3) and similar to that observed for the bis-aromatic CD3938. The third phenyl ring in the side chain is perpendicular to ring 2 and superimposed in all tris-aromatic derivatives complexes (Figure 4A). The same hydrogen bonds forming the anchoring points of the natural ligand are observed for the tris-aromatic complexes through the three hydroxyl groups (Supporting Information Figure 4 and Figure 4A for CD4802). These represent the anchoring points that must be maintained in order to obtain an active conformation. Compared to the bis-aromatic ligands, the tris-aromatic derivatives are more extended, as the distances between the 1-OH group and 3-OH are 15.7 Å for all tris-aromatic ligands and 15.2 Å for the bis-aromatic ones. The hydrophobic interactions of the aromatic rings are similar to those made by the secosteroid rings.

The four tris-aromatic ligands (CD4720, CD4742, CD4802, and CD4849) induce a structural rearrangement of the ligand binding pocket (LBP) that induces a 10% increase of the LBP's volume without altering the agonist feature of VDR. The main differences compared to the previous bis-aromatic derivatives are observed for the side chain that occupies the region of the aliphatic side chain of calcitriol. The substituent in the third phenyl group (propyl in CD4720, CD4849, and CD4842 and ethyl in CD4742) is pointing toward zMet300 in helix H5 without affecting VDR's conformational changes. Compared to calcitriol, additional interactions are observed for the alkyl group in the third phenyl ring, namely, with zIle296 (hIle271) and zMet300 (hMet272) on helix H5 (at 3.5 and 3.3 Å, respectively, for CD4802) (Supporting Information Figure 3). The alkyl chain substituent in the second phenyl (methyl for CD4720 and CD4849 and ethyl for CD4742 and CD4842) points toward zVal328 (hVal300) of helix H6 and induces a displacement of this region in order to accommodate these

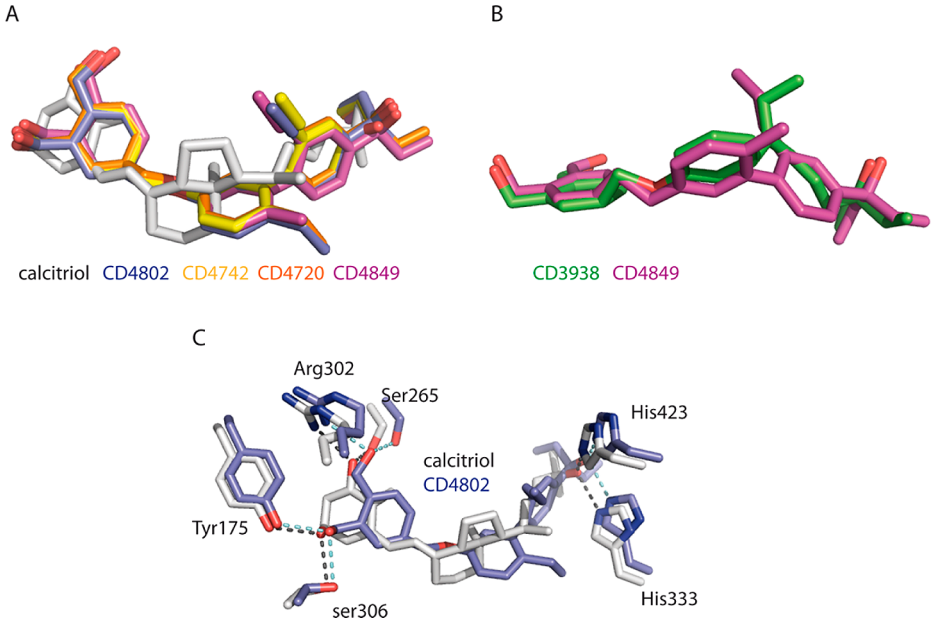

Figure 4. Conformation of the tris-aromatic derivatives. (A) Superimposition of calcitriol (gray) with the tris-aromatic ligands CD4802 (blue), CD4742 (yellow), CD4720 (orange), and CD4849 (magenta) showing that all tris-aromatic derivatives have similar conformations. (B) Superimposition of the bis-aromatic CD3938 (green) and the tris-aromatic CD4849 (magenta). (C) Superimposition of CD4802 (blue) and calcitriol (gray) in the VDR LBP. Hydrogen bonds are shown by dotted lines.

groups. For CD4720 and CD4849, the Cα atoms of zVal328 (hVal300) are shifted by 1−1.5 Å toward the β sheet. For the CD4849 and CD4802, this shift is even larger (close to 2 Å) and helix H6 is moved toward the β-sheet (Figure 5A). Consequently zArg190 is shifted toward the second strand of the β sheet that pushes the loop H1−H3, inducing a displacement of 1 Å of the Cα of zAsp177 (hAsp145) and zSer178 (hSer146). The largest change is observed for CD4802 that exhibits the larger substituent. Compared to calcitriol, additional interactions are also observed with helix H11 (3.7 Å of zLeu440 [hLeu414]) and helix H12 (3.9 Å of zPhe448 [hPhe422]) with the terminal methyl groups.

DISCUSSION AND CONCLUSION

Few nonsecosteroidal compounds have been described as VDR modulators.[12−18,20,21] In the present investigation, we show that the nonsecosteroidal bis-aromatic derivatives (CD4528 and CD3938) and tris-aromatic derivatives (CD4720, CD4742, CD4802, and CD4849) that exhibit similar biological activities as calcitriol in HeLa cells stabilize the VDR LBD in its agonist conformation. One of the tris-aromatic analogues, CD4849, mediates transcription with a magnitude 4-fold higher than the natural ligand. The two or three phenyl rings of the derivatives and their connecting chains mimic the half boat conformation of the bound form of calcitriol. All the important hydrogen bonds forming the anchoring points of calcitriol are maintained by the bis-aromatic and tris-aromatic ligands. These bis- and tris-aromatic analogues are better accommodated by the VDR LBP than the other nonsecosteroidal ligands that have been previously described in the literature as for the VDR complex with YR301, where only four of the six hydrogen bonds of the natural ligand are maintained.[15] Further stability of the bis- and tris-aromatic derivatives is also provided by the hydrophobic van der Waals contacts present in the VDR/1α,25$(OH)_2D_3$ complex and maintained in these new structures. Additional van der Waals contacts are also observed in the complexes formed between VDR and the tris-aromatic analogues, notably with zIle296 (hIle271) and zMet300 (hMet272) in helix H5 and with zLeu440 (hLeu414) in helix H11 and with zPhe448 (hPhe422) in helix H12. For the tris-aromatic analogues, a larger fraction of the LBP is occupied by the ligand, thus giving rise to additional stabilizing contacts compared to the bis-aromatic ligands. In the case of CD4528, additional interactions are mediated through the trifluoromethyl goups. Extension of the alkyl side chains R1 and R2 in the second and third phenyl rings of the tris-aromatic ligands does not affect their transactivation potency. The length of the alkyl group attached to the second phenyl ring that induces some rearrangement of the VDR LBP in the region of helix H6 is not critical and poorly discriminatory in terms of biological activity. Ligand-induced adjustment in the VDR LBP has been previously reported in the structures of the VDR LBD bound to the gemini analogue[29] or to the weak agonists/antagonists 22-butyl-1α,24-dihydroxyvitamin D3 derivatives,[30] where loop H6−H7 and helix H7 is subjected to remodeling (Figure 5B). Here we identify a novel region (helix H6) of the LBP that can be rearranged without affecting the agonistic behavior of the complex. These extended pockets may be important to achieve selectivity and dissociated biological profiles without affecting the agonistic activity of the ligands. The nature of the linker between the first two phenyl rings plays a crucial role in VDR binding affinity. Replacing the oxygen atom from the ether linker to carbon increases the ligand activity. This effect is not due to a difference in conformation or interactions mediated by the two different compounds, as they are similar in CD4849 and CD4720, but to desolvation cost of the ether linker upon VDR binding. Taken together, the structure−function study of bis- and tris-aromatic derivatives with chemical modifications reveals that the higher transcriptional activities are the result of a combination of (i) enthalpic effects through additional and tighter intermolecular contacts due to the higher fraction of LBP being occupied while maintaining

dx.doi.org/10.1021/jm300858s | J. Med. Chem. 2012, 55, 8440−8449

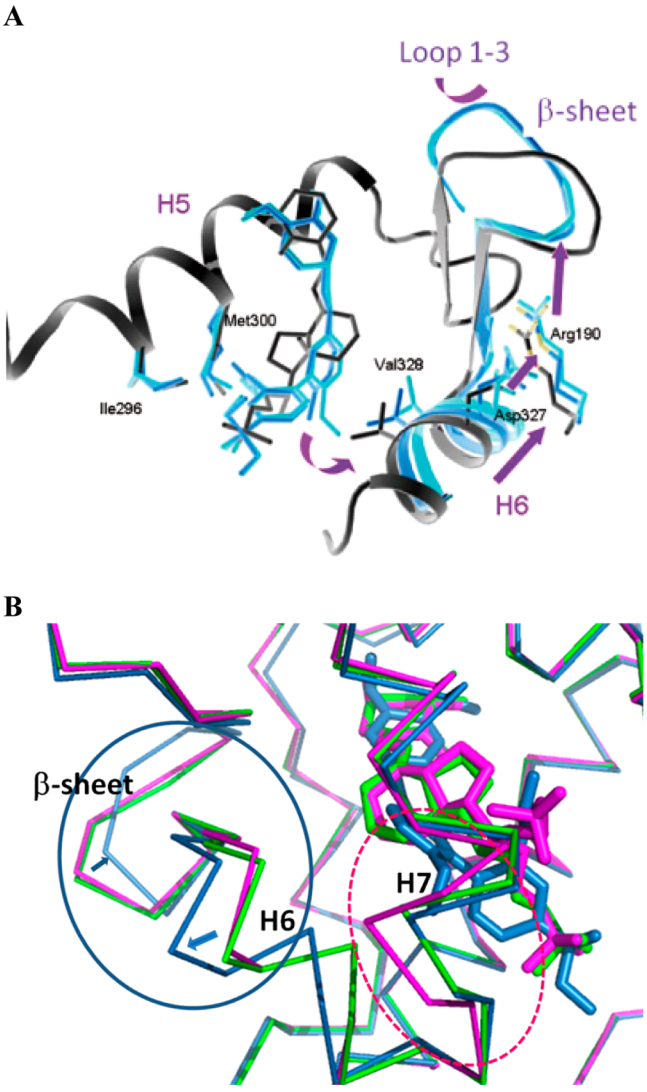

Figure 5. Structural adaptability of VDR ligand-binding pocket. (A) View around the VDR LBP that is subjected to rearrangement induced by the accommodation of the tris-aromatic derivatives CD4849 (blue) and CD4802 (cyan). The VDR/calcitriol is shown in gray. The shifts of the main chain are shown by purple arrows. (B) Comparison of the region remodeled in VDR upon CD4802 binding shown by a blue ellipse and the region remodeled upon gemini binding (pink dashed ellipse). Shown is the superimposition of calcitriol (green), CD4802 (blue), and gemini (pink) in the zVDR LBP.

the hydrogen bond networks and stabilization of helix H12 and (ii) entropic effects with a large contribution of solvation/desolvation.

In summary, this study provides important structure–activity relationship information and contributes to exploration of VDR LBP. The nonsecosteroidal bis- and tris-aromatic analogues with calcitriol-independent molecular scaffold are potent VDR agonists in vitro. The molecular basis for their transcriptional activity is the conservation of the hydrogen binding network and hydrophobic interactions of the natural ligand. As these compounds have structural scaffolds different for the natural ligand, they delineate the general features required for potent VDR activity. Further structure-based design of even more potent and specific ligands on the basis of these structural data can now be considered. Their properties combined with their low calcemic actions make these calcitriol mimics potential drugs to be used in clinical applications.

EXPERIMENTAL SECTION

Compounds. $1\alpha,25(OH)_2D_3$ was purchased from Sigma. The nonsecosteroidal ligands were synthesized by Thibaud Portal and Jean Michel Bernardon (Galderma R&D, Sophia Antipolis, France). All compounds were dissolved in ethanol for a concentration of 10^{-2} M and kept at −20 °C.

Expression, Purification, and Crystallization. The hVDR LBD (118–427Δ166–216) and the zVDR LBD (residues 156–453) were cloned as N-terminal hexahistidine-tagged fusion proteins in pET28b expression vector and overproduced in *E. coli* BL21 DE3 strain. Cells were grown in LB medium and subsequently induced for 12 h at 15 °C with 1 mM isopropyl thio-*β*-D-galactoside. Purification procedure was performed as described in refs 29 and 31 and included an affinity chromatography step on a cobalt-chelating resin. After tag removal by thrombin digestion, the protein was further purified by gel filtration. The final protein buffer was Tris, 10 mM, pH 7.5, NaCl, 150 mM, and DTT, 5 mM. The protein was concentrated to 5–10 mg/mL and incubated with a 3-5 fold excess of ligands and SRC-1 peptide (686-RHKILHRLLQEGSPS-700) in the case of the zVDR. Purity and homogeneity were assessed by SDS and native PAGE as well as denaturant and native electrospray ionization mass spectrometry. Crystals of the zVDR complexes were obtained at 24 °C by vapor diffusion in hanging drops with microseeding method with reservoir solutions containing Bis-Tris, 0.1 M, pH 6.5, lithium sulfate, 1.6 M, and magnesium sulfate, 50 mM. Crystals of hVDR/CD4528 were obtained at 4 °C by vapor diffusion in hanging drops with reservoir solutions containing 0.1 M Mes and 1.4 M ammonium sulfate at pH 6.0.

X-ray Crystallography Data Collection and Processing. The crystals were mounted in fiber loops and flash cooled in liquid nitrogen after cryoprotection with a solution containing the reservoir solution plus 5% glycerol and 2% polyethylene glycol 400 for the crystals of zVDR complexes and 30% glycerol with 5% polyethylene glycol 400 for the crystal of hVDR complex. Data collections from a single frozen crystal for each complex were performed at 100 K at ESRF on ID14-2 beamline or at SLS on PX beamline. Data were integrated and scaled using HKL2000[32] (see statistics in Table 2). A rigid body refinement was used with the structure of the $1\alpha,25(OH)_2D_3$ VDR LBD complex as a starting model. Refinement involved iterative cycles of manual building and refinement calculations. The programs CNS-SOLVE[33] and O[34] were used throughout structure determination and refinement. The ligand molecules were only included at the last stage of the refinement. Anisotropic scaling and a bulk solvent correction were used. Individual *B* atomic factors were refined anisotropically. Solvent molecules were then placed according to unassigned peaks in the difference Fourier maps. Refinement data are summarized in Table 2. Molecular graphics figures were created using Pymol (DeLano Scientific, CA).

Ab Initio Calculations. The structures of all bis- and tris-aromatic ligands presented in Figure 1 were optimized by quantum mechanics. Gaussian 09[35] was used for all ab initio calculations. Geometry optimization was performed at the Hartree–Fock level using the 6-31G* basis set (HF/6-31G*). The initial geometry was obtained from the X-ray data on the complexes with VDR so that the local gas phase minimum closest to the ligand structure in the complex was identified. The geometry and solvation properties of a minimal structure composed of the dibenzyl alcohol (phenyl ring 1) and the second phenyl (ring 2) linked either by an alkyl (base C) or an ether (base O) chain were also investigated. The electrostatic contribution to the desolvation energy of the ligands was computed at the optimized gas phase geometries, using the polarizable continuum model (PCM), in G09. The PCM model is based on a description of the solvent as a macroscopic continuum medium. A dielectric constant of 1 for solute and 78 for solvent was used, and the geometry of the cavity was based on the van der Waals radius of the solute atoms, following the default choice of G09. The solute–solvent interactions are described by a

dx.doi.org/10.1021/jm300858s | J. Med. Chem. 2012, 55, 8440–8449

reaction potential arising from the presence of the dielectric medium[36,37] that interacts with the solute wave function in a self-consistent manner.

■ ASSOCIATED CONTENT

Supporting Information

Four figures showing structures and binding pockets and a table listing volumes of ligands and zVDR LBP. This material is available free of charge via the Internet at http://pubs.acs.org.

■ AUTHOR INFORMATION

Corresponding Author

*Phone: 33.3.88.65.57.81. E-mail: rochel@igbmc.fr.

Present Addresses

[†]NovAlix, Illkirch, France.

[‡]Graduate School of Systems Life Sciences, Kyushu University Graduate School, 6-10-1 Hakozaki, Higashi-ku, Fukuoka 812-8581, Japan.

Notes

The authors declare no competing financial interest.

■ ACKNOWLEDGMENTS

The authors thank Thibaud Portal, Jean Michel Bernardon, Laurent Chantalat, and Bernard Schoot (Galderma R&D, Sophia Antipolis, France) for the bis- and tris-aromatic compounds, Jean-Marie Wurtz for his constructive comments about the manuscript, Sylvie Duclaud and Carole Peluso-Iltis for excellent technical help, André Mitschler and Alastair McEwen for help in data collection, and the staff of the beamlines at ESRF and SLS for experimental assistance during data collection. This study was supported by CNRS, INSERM, Université de Strasbourg, ANR, and Agence de Recherche contre le Cancer (ARC). F.C. was an ARC recipient. Y.C. and A.D. acknowledge generous computer time allocations from Cines and Mesocentre Université de Strasbourg.

■ ABBREVIATIONS USED

NR, nuclear receptor; 1α,25$(OH)_2D_3$, 1α,25-dihydroxyvitamin D_3; LBD, ligand binding domain; VDR, vitamin D receptor; rmsd, root-mean-square deviation

■ REFERENCES

(1) Pike, J. W.; Meyer, M. B.; Bishop, K. A. Regulation of target gene expression by the vitamin D receptor—an update on mechanisms. *Rev. Endocr. Metab. Disord.* **2012**, *13*, 45−55.

(2) Haussler, M. R.; Jurutka, P. W.; Mizwicki, M.; Norman, A. W. Vitamin D receptor (VDR)-mediated actions of 1α,25(OH)2vitamin D3: genomic and non-genomic mechanisms. *Best Pract. Res., Clin. Endocrinol. Metab.* **2011**, *25*, 543−559.

(3) Eelen, G.; Gysemans, C.; Verlinden, L.; Vanoirbeek, E.; De Clercq, P.; Van Haver, D.; Mathieu, C.; Bouillon, R.; Verstuyf, A. Mechanism and potential of the growth-inhibitory actions of vitamin D and analogs. *Curr. Med. Chem.* **2007**, *14*, 1893−1910.

(4) Bouillon, R.; Eelen, G.; Verlinden, L.; Mathieu, C.; Carmeliet, G.; Verstuyf, A. Vitamin D and cancer. *J. Steroid Biochem. Mol. Biol.* **2006**, *102*, 156−162.

(5) Ebert, R.; Schütze, N.; Adamski, J.; Jakob, F. Vitamin D signaling is modulated on multiple levels in health and disease. *Mol. Cell. Endocrinol.* **2006**, *248*, 149−159.

(6) Christakos, S.; DeLuca, H. F. Minireview: Vitamin D: Is there a role in extraskeletal health? *Endocrinology* **2011**, *152*, 2930−2936.

(7) Nagpal, S.; Na, S.; Rathnachalam, R. Noncalcemic actions of vitamin D receptors ligands. *Endocr. Rev.* **2005**, *26*, 662−687.

(8) Hourai, S.; Rodrigues, L. C.; Antony, P.; Reina-San-Martin, B.; Ciesielski, F.; Magnier, B. C.; Schoonjans, K.; Mouriño, A.; Rochel, N.; Moras, D. Structure-based design of a superagonist ligand for the vitamin D nuclear receptor. *Chem. Biol.* **2008**, *15*, 383−392.

(9) Eelen, G.; Valle, N.; Sato, Y.; Rochel, N.; Verlinden, L.; De Clercq, P.; Moras, D.; Bouillon, R.; Muñoz, A.; Verstuyf, A. Superagonistic fluorinated vitamin D3 analogs stabilize helix 12 of the vitamin D receptor. *Chem Biol.* **2008**, *15*, 1029−1034.

(10) Hourai, S.; Rodrigues, L. C.; Antony, P.; Reina-San-Martin, B.; Ciesielski, F.; Magnier, B. C.; Schoonjans, K.; Mouriño, A.; Rochel, N.; Moras, D. Structure-based design of a superagonist ligand for the vitamin D nuclear receptor. *Chem. Biol.* **2008**, *15*, 383−392.

(11) Boehm, M. F.; Fitzgerald, P.; Zou, A.; Elgort, M. G.; Bischoff, E. D.; Mere, L.; Mais, D. E.; Bissonnette, R. P.; Heyman, R. A.; Nadzan, A. M.; Reichman, M.; Allegretto, E. A. Novel nonsecosteroidal vitamin D mimics exert VDR-modulating activities with less calcium mobilization than 1,25-dihydroxyvitamin D3. *Chem. Biol.* **1999**, *6*, 265−275.

(12) Ma, Y.; Khalifa, B.; Yee, Y. K.; Lu, J.; Memezawa, A.; Savkur, R. S.; Yamamoto, Y.; Chintalacharuvu, S. R.; Yamaoka, K.; Stayrook, K. R.; Bramlett, K. S.; Zeng, Q. Q.; Chandrasekhar, S.; Yu, X. P.; Linebarger, J. H.; Iturria, S. J.; Burris, T. P.; Kato, S.; Chin, W. W.; Nagpal, S. Identification and characterization of noncalcemic, tissue-selective, nonsecosteroidal vitamin D receptor modulators. *J. Clin. Invest.* **2006**, *116*, 892−904.

(13) Hakamata, W.; Sato, Y.; Okuda, H.; Honzawa, S.; Saito, N.; Kishimoto, S.; Yamashita, A.; Sugiura, T.; Kittaka, A.; Kurihara, M. (2*S*,2′*R*)-Analogue of LG190178 is a major active isomer. *Mol. Pharmacol.* **2003**, *63*, 211−223.

(14) Kakuda, S.; Okada, K.; Eguchi, H.; Takenouchi, K.; Hakamata, W.; Kurihara, M.; Takimoto-Kamimura, M. Structure of the ligand-binding domain of rat VDR in complex with the nonsecosteroidal vitamin D3 analogue YR301. *Acta Crystallogr., Sect. F: Struct. Biol. Cryst. Commun.* **2008**, *64*, 970−973.

(15) Sato, M.; Lu, J.; Iturria, S.; Stayrook, K. R.; Burris, L. L.; Zeng, Q. Q.; Schmidt, A.; Barr, R. J.; Montrose-Rafizadeh, C.; Bryant, H. U.; Ma, Y. L. A non-secosteroidal vitamin D receptor ligand with improved therapeutic window of bone efficacy over hypercalcemia. *J. Bone Miner. Res.* **2010**, *25*, 1326−1336.

(16) Demizu, Y.; Takahashi, T.; Kaneko, F.; Sato, Y.; Okuda, H.; Ochiai, E.; Horie, K.; Takagi, K.; Kakuda, S.; Takimoto-Kamimura, M.; Kurihara, M. Design, synthesis and X-ray crystallographic study of new nonsecosteroidal vitamin D receptor ligands. *Bioorg. Med. Chem. Lett.* **2011**, *21*, 6104−6107.

(17) Na, S.; Ma, Y.; Zhao, J.; Schmidt, C.; Zeng, Q. Q.; Chandrasekhar, S.; Chin, W. W.; Nagpal, S. A nonsecosteroidal vitamin D receptor modulator ameliorates experimental autoimmune encephalomyelitis without causing hypercalcemia. *Autoimmune Dis.* **2011**, 132958.

(18) Eelen, G.; Verlinden, L.; Bouillon, R.; De Clercq, P.; Muñoz, A.; Verstuyf, A. CD-ring modified vitamin D3 analogs and their superagonistic action. *J. Steroid Biochem. Mol. Biol.* **2010**, *121*, 417−419.

(19) Peräkylä, M.; Malinen, M.; Herzig, K. H.; Carlberg, C. Gene regulatory potential of nonsteroidal vitamin D receptor ligands. *Mol. Endocrinol.* **2005**, *19*, 2060−2073.

(20) Bernardon, J. M. Vitamin D Analogues. World Patent 00/26167, 2000.

(21) Benardon, J. M. Vitamin D Analogues. World Patent 01/38320, 2001.

(22) Chen, F.; Su, Q.; Torrent, M.; Wei, N.; Peekhaus, N.; McMasters, D.; Fisher, J.; Glantschnig, H.; Hodor, P.; Flores, O.; Reszka, A. Identification and characterization of a novel non-secosteroidal vitamin D receptor ligand. *Drug Dev. Res.* **2007**, *68*, 51−60.

(23) Haussler, M. R.; Haussler, C. A.; Bartik, L.; Whitfield, G. K.; Hsieh, J. C.; Slater, S.; Jurutka, P. W. Vitamin D receptor: molecular signaling and actions of nutritional ligands in disease prevention. *Nutr. Rev.* **2008**, *66*, S98−112.

(24) Fink, B. E.; Mortensen, D. S.; Stauffer, S. R.; Aron, Z. D.; Katzenellenbogen, J. A. Novel structural templates for estrogen-receptor ligands and prospects for combinatorial synthesis of estrogens. *Chem. Biol.* **1999**, *6*, 205−219.
(25) Yin, D.; He, Y.; Perera, M. A.; Hong, S. S.; Marhefka, C.; Stourman, N.; Kirkovsky, L.; Miller, D. D.; Dalton, J. T. Key structural features of nonsteroidal ligands for binding and activation of the androgen receptor. *Mol. Pharmacol.* **2003**, *63*, 211−223.
(26) Huang, P.; Chandra, V.; Rastinejad, F. Structural overview of the nuclear receptor superfamily: insights into physiology and therapeutics. *Annu. Rev. Physiol.* **2010**, *72*, 247−272.
(27) Rochel, N.; Moras, D. Ligand binding domain of vitamin D receptors. *Curr. Top. Med. Chem.* **2006**, *6*, 1229−1241.
(28) Rochel, N.; Wurtz, J. M.; Mitschler, A.; Klaholz, B.; Moras, D. The crystal sructure of the nuclear receptor for vitamin D bound to its natural ligand. *Mol. Cell* **2000**, *5*, 173−179.
(29) Huet, T; Maehr, H; Lee, H. J.; Uskokovic, M. R.; Suh, N; Moras, D; Rochel, N. Structure−function study of gemini derivatives with two different side chains at C-20, gemini-0072 and gemini-0097. *MedChemComm* **2011**, *2*, 424−429.
(30) Inaba, Y.; Yoshimoto, N.; Sakamaki, Y.; Nakabayashi, M.; Ikura, T.; Tamamura, H.; Ito, N.; Shimizu, M.; Yamamoto, K. A new class of vitamin D analogues that induce structural rearrangement of the ligand-binding pocket of the receptor. *J. Med. Chem.* **2009**, *52*, 1438−1449.
(31) Rochel, N.; Tocchini-Valentini, G.; Egea, P. F.; Juntunen, K.; Garnier, J. M.; Vihko, P.; Moras, D. Functional and structural characterization of the insertion region in the ligand binding domain of the vitamin D nuclear receptor. *Eur. J. Biochem.* **2001**, *268*, 971−979.
(32) Otwinowski, Z.; Minor, W. Processing of X-ray data collected in oscillation mode. *Methods Enzymol.* **1997**, *276*, 307−326.
(33) Brünger, A. T.; Adams, P. D.; Clore, G. M.; DeLano, W. L.; Gros, P.; Grosse-Kunstleve, R. W.; Jiang, J. S.; Kuszewski, J.; Nilges, M.; Pannu, N. S.; et al. Crystallographic & NMR sytem: a new software suite for macromolecular structure determination. *Acta Crystallogr., Sect. D: Biol. Crystallogr* . **1998**, *54*, 905−921.
(34) Jones, T. A.; Zou, J. Y.; Cowan, S. W.; Kjeldgaard, M. Improved methods for building protein models in electron density maps and the location of errors in these models. *Acta Crystallogr. A* **1991**, *47*, 110−119.
(35) Frisch, M. J.; Trucks, G. W.; Schlegel, H. B.; Scuseria, G. E.; Robb, M. A.; Cheeseman, J. R.; Scalmani, G.; Barone, V.; Mennucci, B.; Petersson, G. A.; Nakatsuji, H.; Caricato, M.; Li, X.; Hratchian, H. P.; Izmaylov, A. F.; Bloino, J.; Zheng, G.; Sonnenberg, J. L.; Hada, M.; Ehara, M.; Toyota, K.; Fukuda, R.; Hasegawa, J.; Ishida, M.; Nakajima, T.; Honda, Y.; Kitao, O.; Nakai, H.; Vreven, T.; Montgomery, J. A., Jr.; Peralta, J. E.; Ogliaro, F.; Bearpark, M.; Heyd, J. J.; Brothers, E.; Kudin, K. N.; Staroverov, V. N.; Kobayashi, R.; Normand, J.; Raghavachari, K.; Rendell, A.; Burant, J. C.; Iyengar, S. S.; Tomasi, J.; Cossi, M.; Rega, N.; Millam, N. J.; Klene, M.; Knox, J. E.; Cross, J. B.; Bakken, V.; Adamo, C.; Jaramillo, J.; Gomperts, R.; Stratmann, R. E.; Yazyev, O.; Austin, A. J.; Cammi, R.; Pomelli, C.; Ochterski, J. W.; Martin, R. L.; Morokuma, K.; Zakrzewski, V. G.; Voth, G. A.; Salvador, P.; Dannenberg, J. J.; Dapprich, S.; Daniels, A. D.; Farkas, Ö.; Foresman, J. B.; Ortiz, J. V.; Cioslowski, J.; Fox, D. J. *Gaussian 09*, revision A.1; Gaussian, Inc.: Wallingford, CT, 2009.
(36) Improta, R.; Scalmani, G.; Frisch, M. J.; Barone, V. Toward effective and reliable fluorescence energies in solution by a new state specific polarizable continuum model time dependent density functional theory approach. *J. Chem. Phys.* **2007**, *127*, 074504.
(37) Improta, R.; Barone, V.; Scalmani, G.; Frisch, M. J. A state-specific polarizable continuum model time dependent density functional theory method for excited state calculations in solution. *J. Chem. Phys.* **2006**, *125*, 054103.